J. Membrane Biol. 159, 83–94 (1997)

The Journal of
Membrane
Biology

Two Different Conductances Contribute to the Anion Currents in *Coffea arabica* Protoplasts

S. Dieudonné*, M.E. Forero, I. Llano**

Laboratorio de Biofísica, Centro Internacional de Física, Edificio Manuel Ancizar, Ciudad Universitaria, Bogotá, Colombia

Received: 25 November 1996/Revised: 9 April 1997

Abstract. The anion conductance of the plasma membrane of *Coffea arabica* protoplasts was isolated and characterized using the whole-cell patch clamp technique. Voltage pulse protocols revealed two components: a voltage-gated conductance (G_s) and a voltage-independent one (G_l). G_s is activated upon depolarization (e-fold activation every +36 mV) with time constants of 1 sec and 5 sec at all potentials. G_l and G_s also differ by their kinetic and biophysical properties. In bi-ionic conditions the current associated with G_s shows strong outward rectification and its permeability sequence is $F^- > NO_3^- > Cl^-$. In the same conditions the current associated with G_l does not rectify and its permeability sequence is $F^- \gg NO_3^- = Cl^-$. Furthermore, at potentials over +50 mV G_s, but not G_l, increases with a time constant of several minutes. Finally the gating of G_s is affected by stretch of the membrane, which leads to an increased activation and a reduced voltage sensitivity. Anion conductances similar to the ones described here have been found in many plant preparations but G_l-type components have been generally interpreted as the background activation of the slow voltage-gated channels (corresponding to G_s). We show that in coffee protoplasts G_l and G_s are kinetically and biophysically distinct, suggesting that they correspond to two different molecular entities.

Key words: Anion channels — Plants — Ionic selectivity — Voltage-dependence — Stretch — Patch clamp

Correspondence to: S. Dieudonné

* *Present address:* Laboratoire de Neurobiologie, Ecole Normale Supérieure, 46 rue d'Ulm, 75230 Paris Cedex 05

** *Present address:* Laboratory of Cellular Neurobiology, Max-Planck-Institut für biophysikalische Chemie, Göttingen, D37077, Germany

Introduction

The most important properties of an ionic conductance are its gating and ionic selectivity. The channels described in the plasma membrane of various higher plant cells can be classified according to their ionic selectivity as nonselective cation channels (Schroeder & Hagiwara, 1990), K^+-selective channels (reviewed in Bentrup, 1990), Ca^{2+}-selective channels (reviewed by Ward, Pei & Schroeder, 1995) and anion channels (reviewed in Tyerman, 1992). The latter constitute a rather large family of ion channels that are suggested to participate in various key cellular functions (Schroeder, 1995).

Several subtypes of anion channels have been defined according to their characteristic gating properties. The first anion channels described in higher plants with electrophysiological methods were stretch-activated channels of tobacco protoplasts (Falke et al., 1988), that were proposed to play a role in turgor regulation and mechanical signal transduction. Voltage-dependent anion channels activated by depolarization were then described in the plasma membrane of guard cells (Keller, Hedrich & Raschke 1989; Schroeder & Hagiwara, 1989). Two subtypes of these channels are expressed by guard cells: fast-activating (R-type) and slow activating (S-type) (Schroeder & Keller, 1992; Linder & Raschke, 1992). Using selective blockers Schroeder, Schmidt & Sheaffer (1993) showed that anion channels constitute the main route for anion efflux during stomatal closure. Many studies have demonstrated physiologically relevant modulation of anion conductances in guard cells. Thus calcium, at micromolar concentrations, constitutively activates anion conductances in the presence of nucleotides (Schroeder & Hagiwara, 1989; Hedrich, Busch & Raschke 1990). Growth hormones as well as malate, which is considered a signal for local pCO_2, modulate the voltage-dependent properties of guard cells anion channels (Marten, Lohse & Hedrich, 1991; Hedrich & Marten, 1993). These modulatory activities in-

volve complex phosphorylation and dephosphorylation cascades (Schmidt et al., 1995). They also involve extracellular sites of modulation recognized by high affinity ligands of the channels (Marten et al., 1992).

Voltage-dependent anion channels have been found in tobacco protoplasts (Zimmermann et al., 1994) and epidermal cells of *Arabidopsis* hypocotyls (Thomine et al., 1995). These studies suggest that anion channels are not only important in the operation of stomata but in other processes yet to be analyzed. In fact, recent evidence indicates that anion channels might be involved in the response of roots to several physiologically relevant stimuli (Schroeder, 1995). In this study, we report the presence of anion conductances in protoplasts of cultured coffee cells. To examine the gating and selectivity of these conductances, ionic conditions were found that allow the complete isolation of the anion currents from contaminating cation or K^+-selective currents. In these conditions, anion currents resembling the S-type currents described by Schroeder & Keller (1992) and the slow-gating anion currents in other preparations could be recorded for more than 30 min in the whole-cell configuration without any washout. Their ionic selectivity, voltage-dependence and stretch-dependence were studied in detail. It is concluded that the global anion conductance represents the sum of two different conductances: a voltage and stretch-dependent slow-gated one (G_l), and a voltage-independent one (G_s).

Material and Methods

Coffee Cell Culture

Partially dedifferentiated calluses were obtained from *Coffea arabica* leaves and grown on a solid medium (Agar-Agar 6.5 $g.l^{-1}$) derived from Murashige and Skoog basal medium (Murashige & Skoog, 1962), supplemented with cistein 30 $mg.l^{-1}$ and necessary hormones. Calluses were split every 20 days and necrotic parts were removed.

Protoplasts Preparation

Protoplasts were obtained by partial digestion of the cell wall followed by osmotic shock. Two to five milligrams of tissue were taken from the callus under sterile conditions and gently triturated in 5 ml of the following medium: Gamborg's medium 3.2 gl^{-1} (lyophilized medium from Sigma), 5 mM $CaCl_2$, 20 mM MES, 0.75% w/v cellulase RS, 0.75% w/v macerozyme, 0.75% w/v cellulase FA, 0.5% w/v B.S.A., adjusted to pH 5.6 with KOH and to 630 mOsmol with mannitol (all enzymes from Onozuka). Digestion was let to proceed for 7 to 10 min at 37°C under mild agitation. After decantation (1 min, room temperature) the supernatant, containing all the protoplasts with a fully digested cell wall, was discarded. The pellet was then washed three times during 5 min in the same solution as above but without enzymes. A pellet was obtained after each wash by centrifugation. At this point, isolated cells with a polygonal shape (due to cell wall remnants) were abundant and they could be kept at 4°C for a whole day. When needed, 100 μl of this sample was put in a poly-L-lysine treated cover glass bottomed chamber. Cells were allowed to adhere for 5 min. The chamber was then perfused with an hypo-osmotic external solution of the following composition (in mM): 10 CsCl, 3 $CaCl_2$, 2 $MgCl_2$, 10 MES, adjusted to pH 5.6 with Trisma base and to 440 mOsm with mannitol. The ensuing osmotic shock liberates the protoplasts from the remaining cell wall. Round, smooth protoplasts were selected for recording.

Patch-Clamp Recording

Unless otherwise indicated, the external solution was the hypo-osmotic solution described above. In some experiments, as indicated in the corresponding figure legends, most of the mannitol was replaced by salt (TEA-Cl 200 mM or TEA-NO_3 200 mM) to increase external anion concentration. Several internal solutions, listed below, were used in this study. Their pH was adjusted to 7.3 with N-Methyl-D-glucamine (NMDG) or with Trisma base. Just before the experiment, the internal solution's osmolarity was adjusted with mannitol to a value 5% inferior to that of the osmolarity of the external solution. In the first section of the results (Fig. 1) the following intracellular solutions were used: solution [a], (mM): 130 TEA-Cl, 70 CsF, 10 EGTA, 1 $CaCl_2$, 10 Hepes; solution [b], (mM): 20 TEA-Cl, 130 H_2SO_4, 130 NMDG, 10 EGTA, 1 $CaCl_2$, 10 Hepes; TNF solution, (mM): 70 TEA-Cl, 70 HF, 70 NMDG, 10 EGTA, 1 $CaCl_2$, 10 Hepes. They will be called by the indicated names in the result section. TNF was the intracellular solution in all the subsequent experiments.

The presence of mM concentrations of F^- or SO_4^{2-} in the internal solutions was necessary to obtain high resistance seals. The use of 10 mM EGTA in the internal solution as well as the relatively low external calcium concentration (3 mM) allowed good control of intracellular calcium levels. The calculated free internal calcium concentration is 10 nM.

Patch pipettes (2–5 MΩ resistance when filled with internal solution [a]) were pulled from borosilicate glass capillaries. Pipette-to-membrane seals of 1–5 GΩ were generally formed in a few minutes by applying gentle, steady suction to the pipette interior. Hyperpolarization of the pipette interior was crucial for fast formation of the seal. The whole-cell configuration was generally obtained by applying large and brief voltage pulses to the pipette (zap). Gentle positive pressure was applied to the inside of the electrode to prevent block of the tip by intracellular organelles. Access resistance (Rs) was maintained under 10 MΩ and ⩾80% of the voltage drop in the electrode was effectively compensated. Under these conditions the voltage error of even large (5 nA) currents is ⩽10 mV. All potentials were corrected for junction potentials. The membrane capacitive transient could be fully compensated, as expected for a spherical cell, ensuring adequate time resolution. The compensated cell capacitance was 9 ± 3 pF (n = 67) for protoplasts of 15–20 μM diameter.

Anionic outward currents of more than 1 nA were generally recorded. As these outward currents are electrically compensated by nonselective currents, such large anionic conductances may produce a change in the ion concentration inside the protoplast. Steady state would be reached when a stable gradient of solutes forms at the pipette tip. This concentration gradient from the pipette to the cell is given by the following equation (Marty & Neher, 1995):

$$\Delta C = J \cdot Rs/(\rho \cdot D)$$

where J is the flux of solutes through the membrane, Rs the access resistance to the cell, ρ the resistivity of the pipette solution and D the diffusion coefficient of the main salt in solution. For a 1 nA current and Rs = 5 MΩ, we obtain a 5 mM salt gradient. As this is less than 5% of the intracellular ion concentration, J has been neglected.

All data were recorded using Axopatch-1D amplifier (Axon instruments), digitized on line at 100–1000 Hz using a Digidata 1200 interface and PClamp6 (Axon Instruments) and analyzed off line using PClamp6 software.

Results

Isolation of Anion Currents

We used the whole-cell configuration of the patch-clamp technique to study the anion conductances present in the plasma membrane of protoplasts isolated from *Coffea arabica.* In a first series of experiments we attempted to block K^+-selective channels by replacing extracellular and intracellular K^+ ions with Cs^+ and TEA^+. To this end, protoplasts were bathed in an extracellular solution containing 10 mM CsCl (osmotic pressure brought to 440 mosm with mannitol; *see* Materials and Methods) and dialyzed with intracellular solutions containing 130 mM TEACl and 70 mM CsF (solution [a] in Materials and Methods). Under these conditions, depolarizing voltage pulses applied from a holding potential of −83 mV produced the activation, at positive potentials, of an outward current (Fig. 1*A*). The reversal potential of the whole-cell current measured at the end of 1-sec voltage pulses was close to +40 mV. Since the Cs^+ equilibrium potential was −50 mV this indicated that anions contributed most of the macroscopic current. However, some current had to be carried by Cs^+ ions since E_{Cl} was above +60 mV and any F^- contribution would have brought the anion reversal potential to even more positive values. The current carried by Cs^+ ions was not further studied.

To isolate the anion conductance, the experiments were repeated after replacing all the internal Cs^+ ions by impermeant cations (TEA^+ and $NMDG^+$; TNF solution, *see* Materials and Methods). In those conditions large currents were required to hold the membrane at hyperpolarized potentials (600 ± 400 pA at −73 mV; $n = 21$). These holding currents developed within a second after initiation of the whole-cell recording configuration, as Cl^- and F^- diffused into the cell. They remained stable for the rest of the experiment. Figure 1*B* presents the current responses to 1-sec voltage pulses applied from a holding potential of −73 mV. Hyperpolarizing pulses gave rise to large instantaneous currents followed by slow relaxations corresponding to the closure of anion conductances. Depolarizing pulses induced relaxations of opposite polarity. The instantaneous *I–V* relation had a reversal potential more positive than +100 mV (Fig. 1*D;* squares) as expected for an anion conductance with $P_F/P_{Cl} > 5.7$ in a Goldman-Hodgkin-Katz (GHK) description of a bi-ionic reversal potential (*see below*).

These presumed anion currents were insensitive to extracellular applications of two classical blockers of anion channels, DIDS (4,4′-diisothiocyanatostilbene-2,2′-disulfonic acid; 10 μM) and IAA-94 ([6,7-dichloro-2cyclo-pentyl-2,3-methyl-1-oxo-1H-indan-5-yl oxy] acetic acid; 10 μM). Nonetheless, replacement of most of the internal anions by the divalent anion sulfate (solution [b] in Materials and Methods) greatly reduced the amplitude of the whole-cell currents (Fig. 1*C;* see *I–V* in Fig. 1*D,* triangles). The holding current at −87 mV dropped to 25 ± 13 pA ($n = 7$), a value ~4% of that of the holding current recorded with a TNF internal solution. This confirms that the whole-cell currents analyzed in this study arise from the flux of monovalent anions.

In some cells, current relaxations with very fast time constants (58 ± 3 msec; $n = 4$) were observed upon repolarization after voltage jumps (*see* Figs. 1*B*,4,5,6). The amplitude of these relaxations was not correlated with that of the anion currents and their apparent reversal potential changed from cell to cell. They may correspond to the tails of currents flowing through channels permeant to external Cs^+ ions, to charge movements from the cytoplasm to the vacuole or to gating charges of

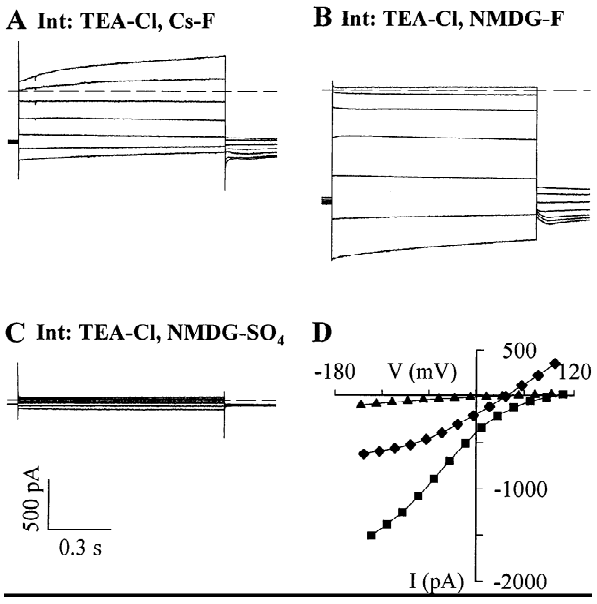

Fig. 1. Whole-cell current-voltage relations of coffee protoplasts in three ionic conditions. Voltage pulses of 1-sec duration are applied from an hyperpolarized holding potential (*Vh;* amplitude of the steps: −60 to 180 mV; steps shown every 40 mV). Dotted lines represent zero current. (*A*) Current traces obtained with a TEACl and CsF based internal solution (internal solution a). Note the presence of outward currents at depolarized potentials. $Vh = -83$ mV. (*B*) Internal Cs^+ was replaced by NMDG (TNF internal solution) leading to the suppression of outward currents. $Vh = -73$ mV. (*C*) Current traces obtained in a different cell when internal monovalent anions were replaced by sulfate (internal solution b). The paucity of internal monovalent anions causes a dramatic reduction of the amplitude of the anion currents. $Vh = -87$ mV. (*D*) Plot of the instantaneous *I–V* relations for the cells shown in *A, B* and *C* (diamonds, squares and triangles respectively).

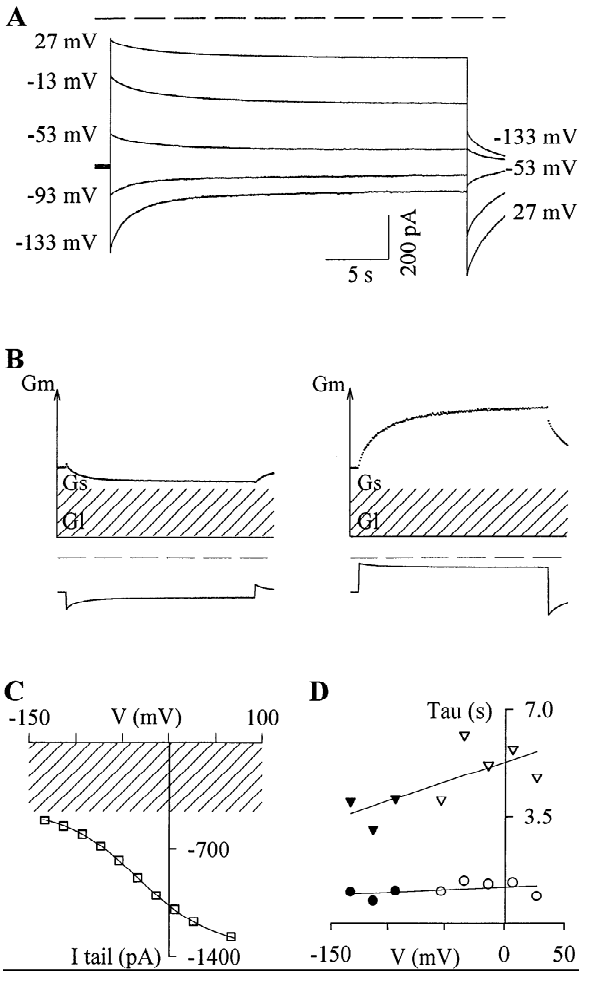

Fig. 2. Voltage dependence of anion currents. Long (30 sec) voltage pulses were used to allow steady state activation of anion currents. (*A*) Whole-cell current traces for pulses to −133, −93, −53, −13 and 27 mV are shown. V_h = 73 mV. TNF internal solution. The interval between voltage pulses was 1 min. Dotted line corresponds to zero current. Biexponential functions fitting the data are superimposed on the current relaxations at all potentials. (*B*) Diagram showing how the total anion conductance can be divided into a voltage-independent component (G_l) and a voltage-dependent one (G_s). The behavior of G_l (dashed area) and G_s (white area) during the most hyperpolarizing and the most depolarizing pulses of Fig. *A* is shown. It can be noted for the depolarizing pulse that a small current relaxation near the reversal potential corresponds to a large change in conductance. (*C*) Instantaneous tail currents measured at the holding potential, 150 msec after the end of the voltage pulse, are plotted against the pulse potential. The steady-state activation curve obtained is fitted by a single Boltzmann function, solid line. The part of the current corresponding to G_l has been dashed. (*D*) Values of the fast and slow time constants of the current relaxations at all pulse potentials. Each point represents the mean of two or three experiments. Filled symbols correspond to deactivation of the anion channels observed during hyperpolarizing voltage pulses. Open symbols correspond to activation time-constants during depolarizing pulses. Solid lines represent the best linear regression. The voltage dependence is 1.7 sec. V^{-1} for the fast time constants and 12.6 sec V^{-1} for the slow time constants.

plasma membrane transporters. Their characterization was not further pursued in this study.

Voltage Dependence of Anion Current

The TNF intracellular solution was used to study the isolated anion currents. As can be seen in Fig. 2*A*, if the holding potential was set to −73 mV these currents showed slow deactivation during hyperpolarizing steps and slow activation when the cell was depolarized. A residual anion current was present even at hyperpolarized potentials. In the rest of the study we will call G_l (for leak conductance) the conductance associated with the hyperpolarization-resistant part of the current. The conductance associated with the depolarization-activated part of the current will be called G_s (to recal its similarity to the slow voltage-gated conductances in other preparations). The behavior of G_s and G_l during hyperpolarizing and depolarizing voltage pulses is schematized in Fig. 2*B*. If the holding potential was set to +47 mV to allow full activation of the voltage-dependent anion conductance, the instantaneous current upon return to −73 mV was 210 ± 35% (n = 4) of the holding current at −73 mV. The voltage-dependent (G_s) and nonvoltage dependent (G_l) components of the conductance are thus of similar amplitude. To this point it is purely conceptual to differentiate those two components. They could arise from the opening of a single molecular entity or from the activity of two different molecular entities. The following study will show that they are indeed different from a biophysical point of view. For sake of clarity, we have chosen to differentiate them from the beginning.

Voltage steps of 30-sec duration allowed the anion current to reach a steady state and were generally used in the rest of the study. Slow tail currents were observed upon return to the holding potential and served to study quantitatively the voltage dependence of the anion conductances. Figure 2*C* shows the *I–V* plot for the tail currents measured at −73 mV, 150 msec after the end of voltage steps. The parts of the tail currents resulting from G_s and G_l activation are indicated. The experimental points were fitted by a single Boltzmann function with a half activation potential of −40 mV and an e-fold dependence on voltage of 39 mV (mean for eight such experiments: 36 ± 10 mV). This shallow voltage dependence is unusual for anion conductances. It contrasts with that found for *R* type channels (threshold to full activation ~50 mV).

Kinetic Properties of G_s

Throughout the range of potentials studied, both the time course of activation and of deactivation were well approximated by the sum of two exponential functions, as illustrated in Fig. 2*A* where the fits are superimposed on

(and indistinguishable from) the current traces. The time constants (τ) obtained are plotted against the pulse potentials in Fig. 2*D*. Each point represents the mean of 2 or 3 experiments. The values for activation τ (opened symbols) and deactivation τ (filled symbols) are very similar and they do not show marked voltage dependence. In the 5 cells analyzed the mean values were 1.4 ± 0.3 sec and 6.2 ± 1.1 sec for the activation process, and 1.2 ± 0.2 sec and 4.2 ± 0.8 for the deactivation process. Deactivation was studied over a larger range of potentials by stepping to a high activating potential (107 mV) for 10 sec and then stepping back to inactivating potentials ranging from −133 to 7 mV (Fig. 3*A*). At all potentials the time course of deactivation could be fitted by two exponentials with time constants close to 1 sec and 5 sec (Fig. 3*B*). The ratio of the amplitude of the two components remained close to 1 for this cell (Fig. 3*C*) but this ratio was very variable from cell to cell. In some cells the fast component was barely detectable whereas in others it could represent 80% of the relaxations.

In all cells studied, the contribution of the fast component was larger in activation relaxations than in deactivation relaxations, suggesting that part of the molecules that undergo fast activation move into a slow state during prolonged depolarization. To test whether fast and slow relaxations represent activation steps of the same molecular entity, their temporal relation was further investigated. Tails were produced by stepping back to the holding potential after depolarizing pulses of varying length (Fig. 4*A*). In a first step, the amplitude of the tails was plotted against the duration of the depolarizing pulses and the resulting activation curve was fitted by two exponentials (time constants of 1.1 sec and 6.3 sec in Fig. 4*B*, squares and corresponding solid line). The fast component in this cell corresponds to 20% of the activation process. In a second step, each tail was fitted by two exponentials. The time constants obtained are plotted in Fig. 4*C*. They are poorly dependent upon the duration of the activation pulse (*see* plotted linear regression) and reasonably close to the activation time constants. The amplitudes of the fast (a1) and slow (a2) components of the tails are plotted in Fig. 4*B*, (circles and triangles respectively), and the ratio a1/a2 is plotted in Fig. 4*D*. The fast component of the tail is predominant for brief activation. Nevertheless it differs from the fast component of the overall activation process (Fig. 4*B*) in that its amplitude is larger than expected for brief activation times and decreases markedly after more than 3 sec of activation. The slow component of the tails becomes gradually more important as the activation of the anion conductance develops but again not as expected from the overall activation. As a result the amplitude of a1/a2 is not well fitted by the ratio of the fast component over the slow component of activation (dashed line in Fig. 4*D*). On the contrary, the relation of a1/a2 to the duration of the activation pulse is well fitted by two exponentials with time constants of 1.1 sec and 6.3 sec (solid line in Figs. 4*D*), in agreement with a simple three state kinetic model where the fast and slow kinetic processes represent sequential activation steps of the same molecular entity (*see* Discussion).

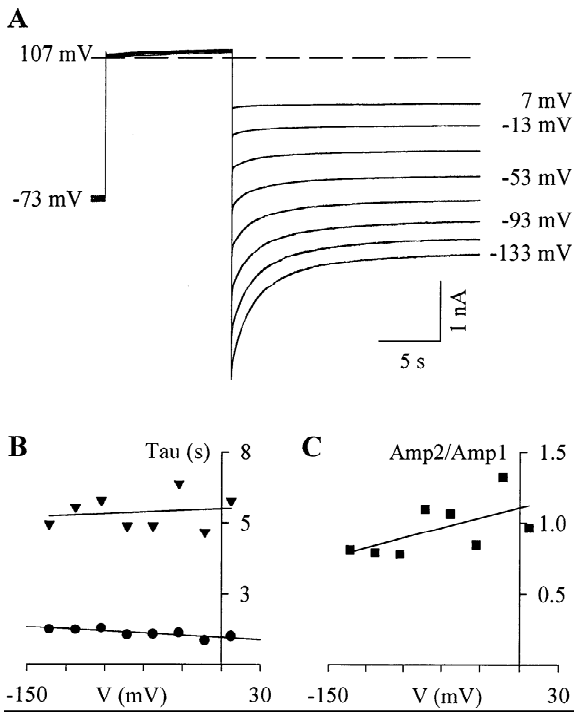

Fig. 3. Voltage-dependence of the deactivation of the anion currents. In these experiments the transmembrane potential was stepped to 107 mV for 10 sec to allow substantial activation of the anion conductances and then stepped back to various potentials, where deactivation can be studied. (*A*) Current traces corresponding to tail potentials ranging from −133 to 7 mV every 20 mV. $Vh = -73$ mV; TNF internal solution. The interval between pulses was 1 min. Doted line corresponds to zero current. The fits by biexponential functions are superimposed on the tail current traces and are almost indistinguishable from them. (*B*) Time constants of tail currents relaxation are plotted against tail potential. Solid lines represent linear regressions. The voltage dependence is −2.5 sec V^{-1} for the fast time constant and 1.9 sec V^{-1} for the slow time constant. (*C*) The ratio between the amplitude of the slow and the fast components is plotted against tail potential. Solid line represents the linear regression (voltage dependence of 2 V^{-1}).

Construction of an i–V Curve

The steady-sate *I–V* relation of an ionic current depends on the voltage-dependence of both the open probability and the single channel current. To characterize separately the latter parameter single channel currents can in principle be measured directly. However, due to the low adherence of the protoplasts to the recording chamber, it was impossible to obtain outside-out patches and al-

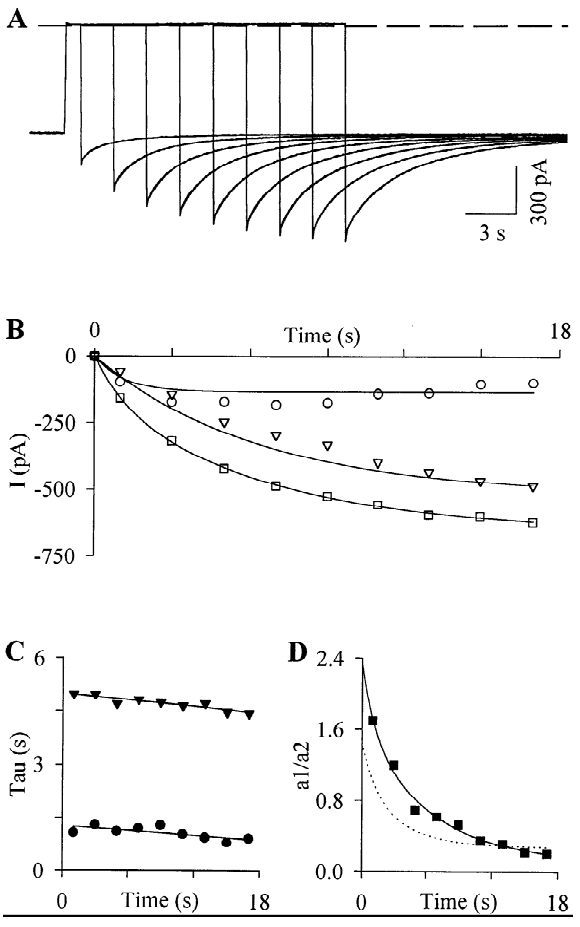

Fig. 4. Relation between fast and slow kinetic components. To see whether successive fast and slow activation are reflected by the respective amplitudes of the fast and slow components of tail deactivation, depolarizing voltage pulses of varying length (first duration 1 sec, increment 2 sec) were applied and the resulting tails were fitted by two exponential functions. (*A*) Current traces corresponding to successive voltage jumps to 107 mV are shown with the fits by biexponential functions superimposed on the tail currents. *Vh* = −73 mV; TNF internal solution. The interval between voltage pulses is 1 min. Dotted line corresponds to zero current. (*B*) Tail current amplitude (open squares), fast exponential component of the tails (open circles) and slow exponential component of the tails (open triangles) are plotted against the duration of the depolarizing voltage pulse. The increase in tail amplitude reflects activation and can be approximated by the sum of two exponentials with time constants 1.1 sec and 6.3 sec (solid line). The fits by two exponential functions (solid lines) are superimposed on data points. (*C*) Time constants for the two exponential functions fitted to the tail currents are plotted against depolarizing pulse duration. Regression lines are superimposed on the data points (regression coefficients 22 msec. sec^{-1} for the fast and 32 msec. sec^{-1} for the slow component). (*D*) The ratio of the amplitude of the fast component over the amplitude of the slow component of the tail is plotted against the duration of the activating voltage pulse. The solid line corresponds to the fit to the data of a double exponential function with time constants 1.1 sec and 6.3 sec. The dashed line represents the fit obtained by dividing the fast exponential component of activation by the slow exponential component of activation, as expected for two independent channels.

though single channel currents were observed in the cell-attached configuration when the pipette was hyperpolarized (patch membrane depolarized), the lack of control of the intracellular medium in that configuration made the interpretation of the data difficult. We therefore used another method to evaluate the voltage dependence of the mean single-channel current for G_s and G_l. This method consists in the normalization of the amplitudes of the currents during and after a voltage jump.

The amplitude (I_a) of the current relaxation seen during a depolarizing voltage pulse, and corresponding to a change in G_s, is given by:

$$I_a\,(V_p) = N \cdot [p_o\,(V_p) - p_o\,(V_h)] \cdot i\,(V_p) \qquad (1)$$

where N is the total number of channels, p_o their open probability, i their single–channel current at the voltage V and V_p and V_h are the test and holding potentials respectively.

The amplitude (I_t) of the relaxation of the tail current upon returning to the holding potential, and corresponding to the opposite change in G_s, is given by:

$$I_t\,(V_p) = N \cdot [p_o\,(V_p) - p_o\,(V_h)] \cdot i\,(V_h) \qquad (2)$$

The tail currents can then be used to normalize the activation current, giving a normalized value of the single channel current at V_p:

$$I_a\,(V_p)/I_t\,(V_p) = i\,(V_p)/i\,(V_h) \qquad (3)$$

This calculation gives an estimate of i for G_s specifically.

At the holding potential the contribution of G_s to the total conductance, is minimal (*see* Fig. 2). Thus, a similar normalized *I–V* relation for G_l can be obtained by dividing the instantaneous pulse current by the holding current.

Permeability of Gs and Gl to Fluoride and Chloride Ions

Figure 5*A* shows current traces elicited by a series of depolarizing pulses and Fig. 5*B* plots $I_a$and I_t as a function of test potential (V_p). The *I–V* relation for the resulting normalized elementary current is plotted in Fig. 5*C*. The reversal potential of the current is more positive than 100 mV (a precise value cannot be obtained due to the small size of the currents around the reversal potential). Given the absence of permeant cations, if Cl^- and F^- had the same permeability the reversal potential would be $58 \cdot \log (200/10) = 75$ mV. We conclude that

F^- is more permeant than Cl^-. The value of P_F/P_{Cl} can be estimated using the GHK equation: $P_F/P_{Cl} > 5.7$. However, the shape of the *i–V* relation deviates from the prediction of the GHK equations (solid line in Fig. 5*C*), suggesting that away from the reversal potential the requirements of the GHK model are not met by the voltage-dependent anion conductance.

To better characterize the relative permeability of the anion conductances to Cl^- and F^-, the external Cl^- concentration was raised to 220 mM using TEA-Cl. Large outward currents were then obtained at positive potentials (Fig. 6*A1*), indicating that external Cl^- ions permeate through these conductances. Figure 6*A2* plots the currents measured at the beginning (mainly due to G_l) and at the end of the pulses ($G_l + G_s$) as a function of the pulse potential. For the total current, the reversal potential was 36 ± 3 mV ($n = 5$, interpolated value). Figure 6*A3* (open circles) shows the elementary *I–V* relation for G_s obtained by the normalization procedure described above (Eq. 3). The curve has an S shape with an inflexion point around the reversal potential and an outward limb much steeper than the inward one. When the GHK equation was used to calculate the relative permeability for F^- over Cl^- from the value of the reversal potential, it yielded a value of $P_F/P_{Cl} = 11.5$. The GHK equations cannot describe the shape of the *I–V* relation over the entire voltage range. Single-site, two-barrier models are usually used to account for S-shaped *I–V* curves. The fit of the data by a biexponential function derived from the simplest form of the single-site model is shown as a solid line in Fig. 6*A3*. The strong outward rectification of i indicates the existence of a conducting state of high amplitude at potentials positive to the reversal potential. This is confirmed by the very high noise level in the corresponding outward current traces.

The *i–V* relationship for G_l was determined as described above (open triangles in Fig. 6*A3*). It also has a sigmoid shape but a slightly more positive reversal potential and a much smaller outward rectification than the *i–V* curve for G_s. Those differences in permeability properties suggest that G_l does not represent the minimal activation of a voltage-dependent conductance (G_s) but is at least a different conducting state.

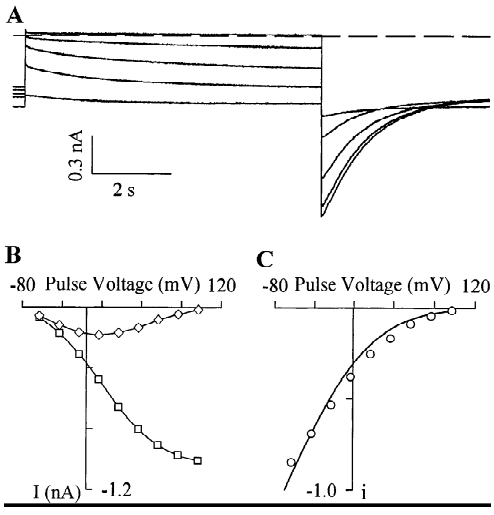

Fig. 5. Construction of an *i–V* curve for the anion conductances. Repeated depolarizing voltage jumps (8-sec duration) of increasing amplitude were applied and activation and tail currents were used to calculate the normalized elementary conductance of the anion channels. (*A*) Current traces for the jumps to −63, −23, 17, 57 and 97 mV are superimposed. TNF internal solution. The interval between voltage pulses was set to 1 min. Dotted line corresponds to zero current. Some instability in the baseline current can be seen and may be explained by the stretch dependence of the anion currents (*see* Fig. 8). (*B*) The amplitude of the activation transient is calculated by subtracting the current amplitude at the end of the voltage pulse from the amplitude at the beginning of the pulse and is plotted against pulse potential (open diamonds). Tail amplitude (open squares) is obtained by subtracting instantaneous tail current from baseline current. (*C*) The elementary current of the channel (*i*) normalized by *i* at the holding potential of −83 mV is calculated from activation and tails amplitudes (*see* text). The resulting normalized *i–V* is plotted. The solid line represents the best fit of the data by a GHK function.

Permeability to Other Anions

Neither Cl^- nor F^- are present at high concentrations in the cytoplasm of plant cells under physiological conditions. We therefore asked whether physiologically relevant anions are permeable through the conductances studied here. We tested NO_3^-, which has been shown to permeate through guard cell anion channels (Keller et al., 1989; Hedrich & Marten, 1993; Schmidt & Schroeder, 1994). Large outward currents were obtained when 200 mM TEA-NO_3 was present in the external solution (Fig. 6*B1*). The interpolated reversal potential of the *I–V* curve (Fig. 6*B2*) was 8 ± 7 mV ($n = 2$), 28 mV more negative than the reversal potential for Cl^- tested in the same conditions. This demonstrates that NO_3^- has a higher permeability than Cl^- through the anion conductances described here. The relative permeability of NO_3^- versus Cl^- is 4.2 and that of NO_3^- *vs.* F^- is 0.36. The first value is very close to that found by Hedrich and Marten (1993) for R-type anion channels (*see also* Keller et al., 1989). Nevertheless the permeability sequence for Cl^-, F^- and NO_3^- differs from the sequence found by Schmidt and Schroeder (1994) for S-type anion channels of guard cells.

The *i–V* curve for G_s was also doubly rectifying with a more pronounced outward rectification. A fit of this curve by the biexponential function derived from a single site model is shown by the solid line in Fig. 6*B3*. Again, the *i–V* curve for the voltage-independent current (open triangles) had a more positive reversal potential and reduced outward rectification.

When glutamate (200 mM) was the anion included in

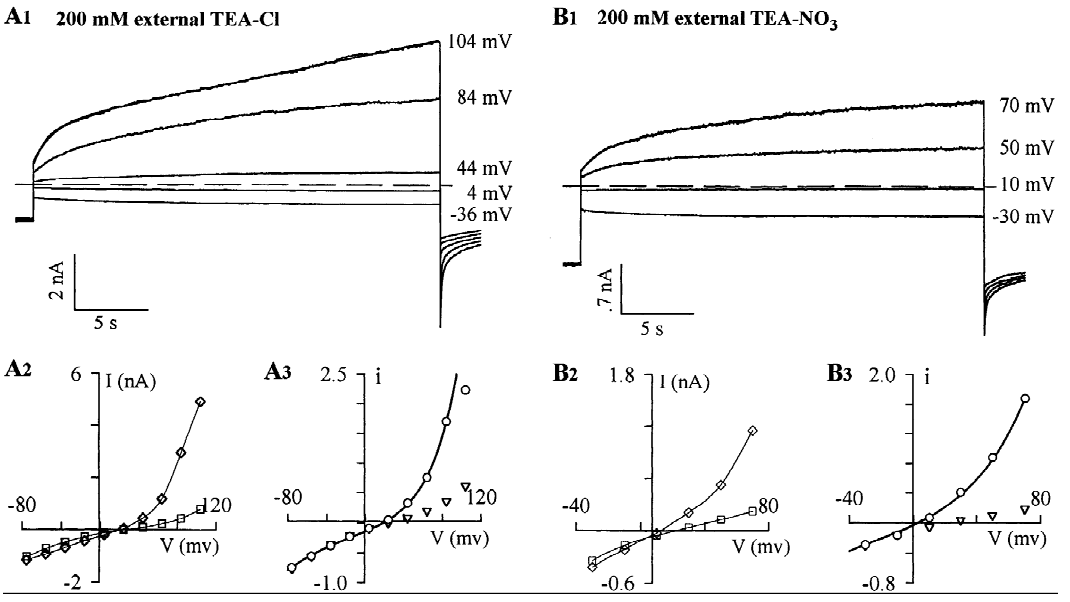

Fig. 6. Relative permeability of the anion conductance to Cl^-, F^- and NO_3^-. Relative permeability of the anion channels to different anions is studied by changing the anions in the external solution. (*A*) 200 mM TEA-Cl were added to the external solution in order to calculate precisely the relative permeability of the anion channels to F^- and Cl^-. (A_1) Current traces elicited by voltage jumps to −36, 4, 44, 84 and 104 mV from a holding of −96 mV. The reversal potential of the current at the end of the pulse is shifted to 25 mV in this cell, and large outward currents carried by external Cl^- ions are seen at more depolarized potentials. The fit by a single exponential function plus a sublinear component is superimposed on the current trace at +84 mV. (A_2) *I–V* curve for the current measured at the beginning (open squares) and at the end (open diamonds) of the voltage jumps. (A_3) Open circles correspond to the *I–V* relation for the voltage activated current, calculated as in Fig. 5. Open triangles represent the *I–V* relation of the holding current, obtained by dividing the current at the beginning of the pulses by the current at the holding potential. Note the different in reversal potential and extent of outward rectification for the two currents. (*B*) 200 mM TEA-NO_3 were added to the external solution to estimate the permeability of NO_3^- ions through the anion channels studied. (B_1) Current traces obtained for voltage jumps to −30, 10, 50 and 70 mV from a holding of −90 mV. The reversal potential is close to 10 mV. Fits by double exponential functions are superimposed on the last two activation transients. (B_2) Same as A_2. (B_3) same as A_3. TNF internal solution. Interval between pulses 1 min. Dotted lines in A_1 and B_1 correspond to zero current.

the external solution no outward current was detected (*data not shown*), demonstrating that large organic zwitterions like glutamate are poorly permeant or impermeant through the anion conductances of coffee protoplasts.

Ultra-slow Activation of G_s at High Positive Potentials

In the presence of external anions, it can be noticed (*see* Fig. 6) that the time course of the outward current is altered at very depolarized potentials: in addition to the components with time constants of 1 sec and 5 sec, activation has a very slow component approximated by a linear function (*see*, e.g., the pulses to +84 and +70 mV in Fig. 6*A1* and 6*B1* respectively). The fast component of the activation process does not change at very positive membrane potentials. In Figs. 6*A1* and 6*B1* the corresponding time constants are 1.1 sec, 1.2 sec and 1.2 sec at +50, +70, and +104 mV respectively. The component of activation with slow time constant cannot be well separated from the linear trend. The amplitude of the linear component (expressed in $pA \cdot min^{-1}$ at +107 mV) was very variable from cell to cell. It was neither correlated to the amplitude of the current at the holding potential (0.3 < relative amplitude < 4.1) nor to the amplitude of the voltage-dependent relaxation at +107 mV (0.6 < relative amplitude < 3.4).

We examined whether the slow activation of the anion conductance at very depolarized potentials could be produced in the absence of external anions. To do so, voltage steps of increasing length (to +67 or +107 mV) were given every minute in the low Cl^- external solution (Fig. 7*A*). The amplitude of the tail currents was measured and plotted against the duration of the test pulse, as in Fig. 4. A very slow activation can already be seen after 15 sec at +67 mV (open squares in Fig. 7*B*). At +107 mV the slow activation was marked (filled squares in Fig. 7*B*). Thus, slow activation also occurs in the absence of external anions.

If the previous protocol is applied in the presence of external anions (200 mM TEA-NO_3, Fig. 7*C*) the activation of the voltage-dependent current can be followed at positive potential for each of the successive pulses. Figure 7*D* illustrates that the amplitude of the voltage-dependent component increased from pulse to pulse whereas the amplitude of the voltage-independent

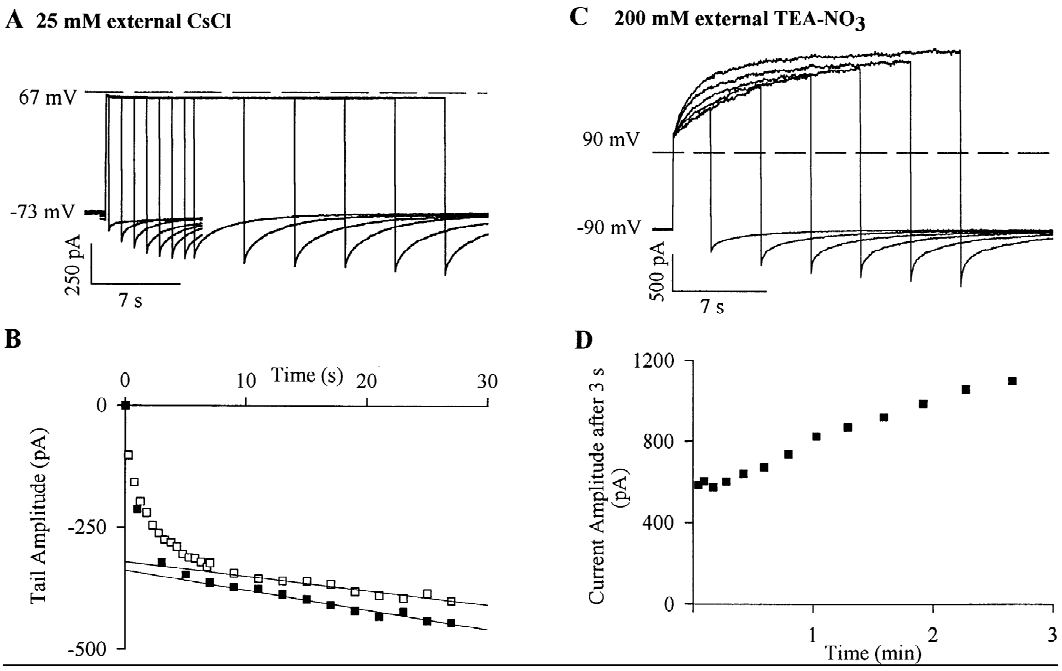

Fig. 7. Study of the very slow activation of anion conductances at high depolarized potentials. Tail currents were used to determine if the very slow activation occurs in the absence of external anions. (*A*) Voltage pulses of increasing duration were applied every 1 min. The current traces corresponding to 0.5 sec first pulse duration, increment 1 sec for the first eight pulses and 3 sec for the last five, were superimposed. (*B*) The tail amplitudes are plotted against the duration of the voltage jump for test potentials of 7 mV (open squares) and 107 mV (filled squares). The straight lines indicate the linear regression for the last 6 points (17 sec to 27 sec of activation). They represent the amplitude of the very slow activation after the 1 sec and 5 sec components of activation have proceeded. The regression coefficients are -2.9 pA.sec^{-1} at 67 mV and -4.0 pA.sec^{-1} at 107 mV. (*C*) The experiment was repeated in the presence of external anions (NO_3^-) to see if the slow activation is cumulative in a protocol of repeated depolarization or if it comes back to the original equilibrium during the 1-sec interval between pulses. Traces show clearly that the amplitude of the fast activation at test potential (90 mV) gets bigger from pulse to pulse (first trace corresponds to 3 sec activation and the increment is 3 sec). This suggests that the channels once activated by the very slow activation process fall into the pool of the fast activating channels. (*D*) This phenomenon is clearly shown when plotting the amplitude of the activation transient after 3 sec against the cumulated time spent at +90 mV since the beginning of the protocol. TNF internal solution. Dotted lines in *A* and *C* correspond to zero current.

conductance was not changed by the slow activation process.

In Fig. 7*D* the amplitude of the outward current at 90 mV is plotted against the total time spent at 90 mV during successive pulses. From this plot, it is estimated that the amplitude of the voltage-dependent conductance can increase as much as 100% in ~3 min. It can be concluded that the very slow conductance increase at positive potentials reflects the recruitment of new molecules underlying G_s but not G_l. Upon repolarization these molecules do not return to their initially inactive state but rather to the ''immediately available'' voltage-gated state, from which they can be activated with time constants of 1 sec and 5 sec.

Stretch-dependence of the Anion Conductances

When the potential was maintained at −73 mV, inward currents in the nanoampere range were generally recorded. These currents are selectively carried by internal anions leaving the intracellular space through the resting membrane conductances. They are balanced by a non-selective current injected into the cell through the pipette. Although cations in the intracellular solution have a diffusion constant inferior to that of anions, they will nevertheless carry a substantial fraction of the current and thus lead to a net loss of salt by the cell (*see* Materials and Methods). This loss is in turn balanced by passive diffusion of water from the cell (towards the pipette and towards the extracellular solution) leads to continuous shrinkage of the protoplast. This phenomenon was indeed observed. To prevent it, most experiments were performed while applying a positive hydrostatic pressure to the pipette. This pressure was adjusted to eliminate cell shrinkage without inflating the protoplast.

In a separate set of experiments we took advantage of the possibility of changing the volume of the protoplast to study the stretch dependence of the anion conductances. In these experiments stretch was produced by applying a strong positive pressure to the pipette at the same time a short high-voltage pulse was produced to

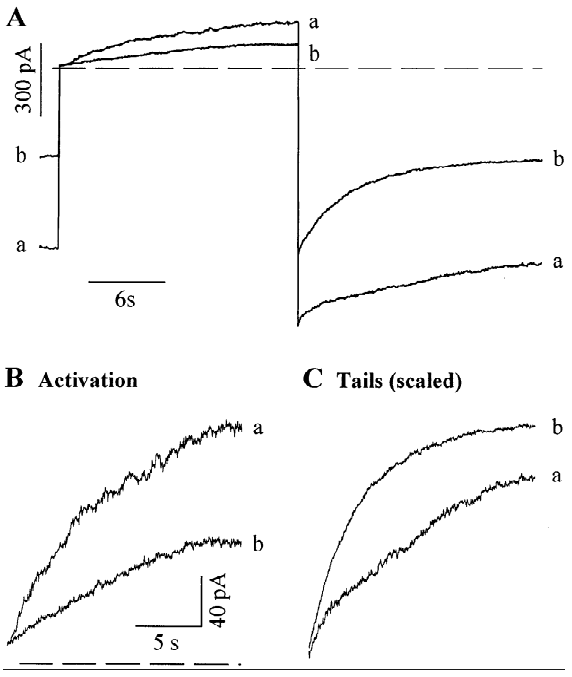

Fig. 8. Stretch dependence of the anion conductances. (*A*) When the whole-cell recording configuration is established while applying a steady positive pressure to the pipette, the protoplast can be kept in a stretched state. Trace a shows the current during and after a pulse from −73 to 107 mV in those conditions. Subsequent release of most of the positive pressure allows slight shrinkage of the protoplast and releases all the stretch on the protoplast membrane (experimental conditions used in all previous experiments shown). Trace b shows the current recorded for the same voltage pulse as in a. The holding current is doubled by stretch. At the same time the activation current during the pulse is increased but the tail current is reduced. (*B*) Plot of the activation currents at an expanded amplitude scale. (*C*) Plot of the scaled tail currents to show that stretch slows the deactivation. TNF internal solution. Dotted lines in *A* and *B* correspond to zero current.

enter the whole-cell configuration. Trace a in Fig. 8*A* shows the behavior of the current in a stretched state (i.e., positive pressure maintained in the pipette) during and after a pulse from −73 to +107 mV. When the positive pressure was removed, cell shrinkage occurred and the amplitude of the holding current decreased gradually, reaching 50 ± 9% of its initial value within a few minutes ($n = 3$). This phenomenon, which is illustrated in trace b of Fig. 8*A*, was partially reversed by applying positive pressure to the pipette, indicating that the reduction of holding current was not linked to a washout of the anion conductance but to its stretch sensitivity. Apart from increasing the amplitude of the holding current, the stretch of the membrane slows down the tail current associated with the deactivation of G_s and decreases its amplitude (Fig. 8*C*). Put together, these results suggest that stretch promotes the activation of G_s at hyperpolarized potentials, leading to an apparent increase of G_l at the holding potential. This issue will be addressed in the kinetic model developed in the discussion.

A paradoxical effect is seen at depolarized potentials. Outward current relaxations are increased by stretch (and not reduced like the tails). Figure 8*B* displays, on an expanded amplitude scale, the current during the pulse to +107 mV. The onset of the traces corresponds to the beginning of the pulse. The amplitude of the instantaneous current (corresponding mainly to the baseline and leak currents at this potential) is similar in the stretched and nonstretched conditions. The kinetics of activation is similar to that of the currents recorded so far at these potentials (e.g., Figs. 6 and 7) but the outward rectification is increased upon stretch. When external anions were present, stretch also caused a dramatic increase in the amplitude of the outward current relaxations during depolarizing pulses. This effect is easily explained if the conductance substate favored by stretch presents a strong outward rectification (which seems to be the case when it is activated by depolarization, *see* Fig. 6). Voltage activation of a reduced number of molecules (as shown by the decrease in tail amplitude) would then result in more outward current (high elementary conductance).

Discussion

In this work we describe a new plant cell preparation in which large voltage-dependent anion conductances can be measured. In previous studies concerning anion conductances the use of Cs^+ ions in the external and internal solutions had been assumed to block the voltage-dependent K^+ channels. However we show that, in coffee protoplasts, the exclusive use of large impermeant cations is necessary to completely block the cationic conductances. The use of such cations allowed the recording of pure anion currents and the study of their voltage dependence and of their ionic selectivity. Another peculiarity of this work is the use of internal solutions containing millimolar concentrations of F^- and no added ATP. Anion currents recorded in these conditions are kinetically very similar to S-type anion currents described in guard cells (Schroeder & Keller, 1992; Schroeder, Schmidt & Sheaffer, 1993) and in tobacco protoplasts in the absence of ATP or in the presence of staurosporine, a protein kinase inhibitor (Zimmermann et al., 1994). We did not observe any rundown in our experiments, probably due to the presence of F^- which is well known to inhibit dephosphorylation processes. In view of the homogeneity and stability of the recordings obtained in this work, F^--containing internal solutions may prove useful to study the properties of slow anion currents in various plant cell preparations.

Previous studies have shown that the relative permeabilities for the halide followed Eisenman series I

(Hedrich & Marten, 1993), suggesting anion binding sites of low field strength within the pore. The *I–V* curves obtained in this work confirm the existence of a site of permeation inside the channel. We also found a value for the relative permeability for NO_3^- over Cl^- very close to that found by Hedrich & Marten. Nevertheless, unlike GABA-gated or glycine-gated channels of mammalians which do have a site of low field strength in the pore (Bormann, Hamill & Sakmann, 1987), plant anion channels have a high permeability to F^-. This suggests the existence of specific binding interactions inside the pore of plant anion channels. Given the structural similarity between O^- groups and F^- ions and the unexpectedly high permeability of NO_3^- through these channels, we propose the existence of a selectivity site for molecules containing O^- groups such as small organic acids.

The properties of the anion conductances presented in this work suggest the presence of both a constitutive (voltage-independent) component, G_l, and a voltage-dependent component, G_s. It is shown in Fig. 6 that these two components differ both in their relative permeability to different anions and in the extent of their outward rectification. Such differences can be explained either by the presence of two different channel types or by the existence of two open states of the same channel, each with distinct permeation properties. These open states would be in voltage-dependent equilibrium, the outwardly rectifying state being favored by depolarization. The experiments illustrated in Fig. 7 prove that such is not the case. Ultra slow activation (occurring at potentials more positive than +60 mV) can double the amplitude of G_s without affecting the amplitude of G_l. No equilibration between the two types of conductances is seen during the 15-min duration of the experiment. G_s and G_l are kinetically separated and therefore probably represent the activity of two different molecular entities.

Channels described by others as rapidly gated by the membrane voltage may participate to G_l in our preparation. Indeed, several authors have shown that modulation of the R-type channels by ATP and/or phosphorylation is characterized by a shift in the peak of activation towards more hyperpolarized potentials (Marten et al., 1991; Marten et al., 1992; Hedrich & Marten, 1993; Zimmermann et al., 1994; Thomine et al., 1995). According to Thomine et al. (1995) intracellular ATP and/or dephosphorylation control the transition from a fast-gating mode into a slow-gating mode of the same molecular entity (*see also* Zimmermann et al., 1994). In the work of Thomine et al., full activation is already obtained at −150 mV in the absence of internal ATP. If the scheme proposed by Thomine et al. was applicable to coffee cells, a constitutive and voltage-independent part of the anion conductance in our work could correspond to the R-type current. We propose therefore that absence of ATP leads to full activation of R-type channels at potentials positive to −150 mV (G_l).

A simple kinetic model can be developed for the channels underlying G_s. Equilibration between at least three states is required to account for the two time constants of activation and deactivation:

$$\text{Closed} \rightleftharpoons \text{B} \rightleftharpoons \text{C}$$

It has been shown in Fig. 4 that channels first enter the fast–gating kinetic state and subsequently reequilibrate slowly into the slow–gating kinetic step. The fast and voltage–dependent gating step must therefore precede the slow–gating step, leading to a scheme with two open states:

$$\underset{}{\text{Closed}} \rightleftharpoons \underset{\substack{\tau = 1\ \text{sec;}\\ \text{V-dependent}}}{\text{Open 1}} \rightleftharpoons \underset{\substack{\tau = 5\ \text{sec;}\\ \text{V-independent}}}{\text{Open 2}}$$

As the proportion of the fast and slow components of the tail is the same at all potentials, the transition between the first and the second open states has to be voltage–independent. In this model, constitutive activation by stretch is easily explained if stretch displaces the equilibrium towards the second open state. This would also lead to a reduction of the number of channels available for activation by voltage, and therefore to the observed reduction in tail current amplitude. Furthermore, the *I*–V plots indicate that at least one of the open states activated by the voltage has a high permeability to external anions (outward rectification). The paradoxical outward rectification produced by stretch can be explained if the second open state is the outward rectifying state. The final scheme then becomes:

$$\underset{}{\text{Closed}} \rightleftharpoons \underset{\substack{\tau = 1\ \text{sec;}\\ \text{V-dependent}\\ \text{stretch-independent}}}{\text{Open 1}} \rightleftharpoons \underset{\substack{\tau = 5\ \text{sec;}\\ \text{V-independent}\\ \text{stretch-dependent}}}{\underset{\text{(outward rectifying)}}{\text{Open 2}}}$$

The functional role of the anion channels in plant cells other than guard cells can be discussed. The S-type channels resemble the outwardly rectifying anion channels found in roots (Skerrett & Tyerman, 1994). Those channels have been proposed to play a role in low affinity NO_3^- uptake into root tissue. The S-type conductance described here (G_s) could play a similar role (for a review on NO_3^- movements in plants *see* Clarkson, 1986). It could also play a role in turgor regulation. When the cell is hyperosmotic compared to the external medium it would become turgescent and the S-type channel would be activated by stretch, providing a path for anion

extrusion from the cell. The fact that in other preparations slow-gated voltage-dependent anion channels are modulated by ATP indicates that they could also play a role in metabolic processes. Regulation of K^+ channels by photosynthetically produced ATP has also been shown in *Arabidopsis* (Spalding & Goldsmith, 1993). In the case of a nonphotosynthetic cell, ATP concentration depends on the organic energetic supply of the cell. Low ATP concentrations may lead to the constitutive activation of R-type channels. Those channels will depolarize the membrane to values close to the Cl^- equilibrium potential, activating in turn the S-type channels and K^+ channels. S-type channels could then provide a path for the entry in the cell of anion metabolites. Restored levels of ATP would bring the cell back to the initial situation. Such slow and spontaneous membrane potential oscillations have already been described in plant cells (Gradmann, Blatt & Thiel, 1993; for a review *see also* Davies, 1987).

We thank P. Ascher, A. Barbier-Brygoo, J. Guern, A. Marty and S. Thomine for their comments on the manuscript. This project was financed by grants from the European Community (No. CI1-CT91-0874) and by the Colombian Institute for Science and Technology (COLCIENCIAS).

References

Bentrup, F.W. 1990. Potassium ion channels in the plasmalemma. *Physiologia Plantarum* **79:**705–711

Bormann, J., Hamill, O.P., Sakmann, B. 1987. Mechanism of anion permeation through channels gated by glycine and γ-aminobutyric acid in mouse cultured spinal neurones. *J. Physiol.* **385:**243–286

Clarkson, D.T. 1986. Regulation of the absorption and release of nitrate by plant cells: A review of current ideas and methodology. *In:* Fundamental, Ecological and Agricultural Aspects of Nitrogen Metabolism in Higher Plants. H. Lambers, J.J. Neeteson, and I. Stulen, editors. Martinus Nijhoff, Netherlands.

Davies, E. 1987. Action potentials as multifunctional signals in plants: a unifying hypothesis to explain apparently disparate wound responses. *Plant, Cell and Environment* **10:**623–631

Falke, L.C., Edwards, K.L., Pickard, B.G., Misler, S. 1988. A stretch-activated anion channel in tobacco protoplasts. *FEBS Lett.* **237:**141–144

Gadsby, D.C., Nairn, A.C. 1994. Regulation of CFTR channel gating. *Trends in Biological Sciences* **19:**513–518

Gradmann, D., Blatt, M.R., Thiel, G. 1993. Electrocoupling of ion transporters in plants. *J. Membrane Biol.* **136:**327–332

Hedrich, R., Busch, H., Raschke, K. 1990. Ca^{2+} and nucleotide dependent regulation of voltage dependent anion channels in the plasma membrane of guard cells. *EMBO J.* **9:**3889–3892

Hedrich, R., Marten, I. 1993. Malte-induced feedback regulation of plasma membrane anion channels could provide a CO_2 sensor to guard cells. *EMBO J.* **12:**897–901

Keller, B.U., Hedrich, R., Raschke, K. 1989. Voltage-dependent anion channels in the plasma membrane of guard cells. *Nature* **341:**450–453

Linder, B., Raschke, K. 1992. A slow anion channel in guard cells, activating at large hyperpolarization, may be the principal for stomatal closing. *FEBS Lett.* **313:**27–30

Marten, I., Lohse, G., Hedrich, R. 1991. Plant growth hormones control voltage-dependent activity of anion channels in plasma membrane of guard cells. *Nature* **353:**758–762

Marten, I., Zeilinger, C., Redhead, C., Landry, D.W., AL-Awqati, Q., Hedrich, R. 1992. Identification and modulation of a voltage-dependent anion channel in the plasma membrane of guard cells by high-affinity ligands. *EMBO J.* **11:**3569–3575

Marty, A., Neher, E. 1995. Tight-seal whole-cell recording. *In:* Single-Channel Recording, second edition. B. Sakmann and E. Neher, editors. pp. 31–52. Plenum Press, New York

Murashige, T.S., Skoog, F. 1962. A revised medium for a rapid growth and bioassays with tobacco tissue cultures. *Physiologia Plantarum* **15:**473–497

Schmidt, C., Schelle, I., Liao, Y.-J., Schroeder, J.I. 1995. Strong regulation of slow anion channels and abscisic acid signaling in guard cells by phosphorylation and dephosphorylation events. *Proc. Nat. Acad. Sci. USA* **92:**9535–9539

Schmidt, C., Schroeder, J.I. 1994. Anion selectivity of slow anion channels in the plasma membrane of guard cells. *Plant Physiol.* **106:**383–391

Schroeder, J.I. 1995. Anion channels as central mechanisms for signal transuction in guard cells and putative functions in roots for plant-soil interactions. *Plant Mol. Biol.* **28:**353–361

Schroeder, J.I., Hagiwara, S. 1989. Cytosolic calcium regulates ion channels in the plasma membrane of *Vicia faba* guard cells. *Nature* **338:**427–430

Schroeder, J.I., Hagiwara, S. 1990. Repetitive increases in cytosolic Ca2+ of guard cells by abscisic acid activation of nonselective Ca2+ permeable channels. *Proc. Natl. Acad. Sci. USA* **87:**9305–9309

Schroeder, J.I., Keller, B.U. 1992. Two typees of anion channel currents in guard cells with distinct voltage regulation. *Proc. Natl. Acad. Sci. USA* **89:**5025–5029

Schroeder, J.I., Schmidt, C., Sheaffer, J. 1993. Identification of high-affinity slow anion channel blockers and evidence for stomatal regulation by slow anion channels in guard cells. *The Plant Cell* **5:**1831–1841

Skerrett, M., Tyerman, S.D. 1994. A channel that allows inwardly directed fluxes of anions in protoplasts derived from wheat roots. *Planta* **192:**295–305

Spalding, E.P., Goldsmith, M.H.M. 1993. Activation of K^+ channels in the plasma membrane of arabidopsis by ATP produced photosynthetically. *The Plant Cell* **5:**477–484

Thomine, S., Zimmermann, S., Guern, J., Barbier-Brygoo, H. 1995. ATP-dependent regulation of an anion channel at the plasma membrane of protoplasts from epidermal cells of arabidopsis hypocotyls. *The Plant Cell* **7:**2091–2100.

Tyerman, S.D. 1992. Anion channels in plant cells. *Annu. Rev. Plant Physiol. Plant Mol. Biol.* **43:**351–373

Ward, J.M., Pei, Z-M., Schroeder, J.I. 1995. Roles of ion channels in initiation of signal transduction in higher plants. *The Plant Cell* **7:**833–844

Zimmermann, S., Thomine, S., Guern, J., Barbier-Brygoo, H. 1994. An anion current at the plasma membrane of tobacco protoplasts shows ATP-dependent voltage regulation and is modulated by auxin. *The Plant J.* **6:**707–716